Materials and Design 192 (2020) 108664

Contents lists available at ScienceDirect

Materials and Design

journal homepage: www.elsevier.com/locate/matdes

Theoretical study of active Ca element on grain refining of carbon-inoculated Mg-Al alloy

Shu-Qing Yang [a], Cheng-Bo Li [a], Jun Du [a,*], Yu-Jun Zhao [b,c,**]

[a] School of Materials Science and Engineering, South China University of Technology, Guangzhou 510640, China
[b] Department of Physics, South China University of Technology, Guangzhou 510640, China
[c] Key Laboratory of Advanced Energy Storage Materials of Guangdong Province, South China University of Technology, Guangzhou 510640, China

HIGHLIGHTS

- Al_2MgC_2 and Al_4C_3 particles are more easily to adsorb around molten Mg due to the adsorption of Ca.
- The doping of Ca makes Mg/Al_2MgC_2 and Mg/Al_4C_3 interfaces more stable.
- Ca could effectively migrate from first-layer to the second-layer in the initial nucleating stage.
- The size of Al_2MgC_2 and Al_4C_3 particles.

GRAPHICAL ABSTRACT

Ca is easier to adsorb on Al_2MgC_2 and Al_4C_3 surfaces, and then promote the subsequent adsorption of Mg. For the Al_2MgC_2 and Al_4C_3 particles with radius (r_{K1}) slightly smaller than the critical nucleation radius r_K, there are chances that their size beyond r_K after the adsorption, and thus enhancing the nucleation rate.

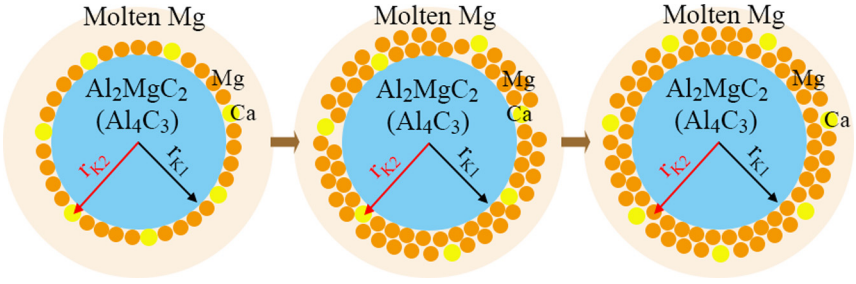

ARTICLE INFO

Article history:
Received 13 February 2020
Received in revised form 11 March 2020
Accepted 20 March 2020
Available online 21 March 2020

Keywords:
First-principles calculation
Heterogeneous nucleation
Mg-Al alloy
Critical nucleation radius
Interfacial properties

ABSTRACT

It is crucial to study grain refinement and refinement mechanism for promoting mechanical properties of Mg alloys. In this work, the influence mechanism of Ca on the grain refinement of Al_2MgC_2 and Al_4C_3 in Mg alloys was studied. It shows that Ca is easier to adsorb on the surfaces of Al_2MgC_2 and Al_4C_3 particles than Mg, which further promotes the adsorption Mg on the surfaces of Al_2MgC_2 and Al_4C_3 particles, leading to more crystal nuclei beyond the critical nucleation radius r_K. The interface of Ca replaced Mg-2 is found to be more stable, for both Mg/Al_2MgC_2 interface and Mg/Al_4C_3 interface. We further revealed that Ca could effectively migrate from the first-layer to the second-layer in both the adsorption slabs and doped interface slabs under ambient condition.

* Correspondence to: J. Du, Department of Metallic Materials, School of Materials Science and Engineering, South China University of Technology, 381 Wushan Rd, Guangzhou, Guangdong 510640, China.
** Correspondence to: Y-J. Zhao, Department of Physics, South China University of Technology, 381 Wushan Rd, Guangzhou, Guangdong 510640, China.
E-mail addresses: tandujun@sina.com (J. Du), zhaoyj@scut.edu.cn (Y.-J. Zhao).

https://doi.org/10.1016/j.matdes.2020.108664

1. Introduction

Magnesium alloys have various advantages in modern industries with a wide application [1,2], due to its low density, high specific strength, good electromagnetic shielding properties and excellent recyclability [3,4]. However, magnesium alloys also have some disadvantages that cannot be ignored, such as low tensile strength and low mechanical properties [5]. According to Hall-Patch formula $\sigma_y = \sigma_0 + Kd^{-1/2}$, the mechanical properties of magnesium alloys will be improved significantly if the grain of magnesium alloys is effectively refined [6]. In the studies of grain refining of metals and alloys, one of the popular theory of metal crystallization nucleation is heterogeneous nucleation ($\sigma_{LB} = \sigma_{\alpha B} + \sigma_{\alpha L}\cos\theta$) [7]. The carbon inoculation method was proved to be an effective method to refine the grain of Mg—Al alloys [8–10] following the heterogeneous nucleation mechanism, which is essentially an interface problem. According to experimental researches, the Al_4C_3 and Al_2MgC_2 heterogeneous nucleation have proved to be the grain refining mechanism of Mg—Al alloys by carbon inoculation [11,12].

The interfacial problem in the nucleation process has been studied for many years, and the theory of low misfit mechanism was developed [13–15]. In 1952, Turnbull and Vonnegut proposed Turnbull-Vonnegut empirical formula $\delta = \Delta a/a_0$ [13], suggesting that the nucleation is effective if $\delta \leq 0.005$ to 0.015. In 1970, Brimfitt model [14] was proposed to define the misfit between planes of the interface. In 1998, Zhang and Kelly proposed the E2EM (edge-to-edge matching) model [15], demonstrating that the effective nucleation should meets $f_r = \frac{r_m - r_p}{r_m} < 10\%$ and $f_d = \frac{d_m - d_p}{d_m} < 6\%$. Nowadays, in-depth study of the refinement mechanism goes deep into the atomic level, and thus it is difficult to study only by experiments and theory. At the same time, the computational simulation is increasingly used in materials research as it can study the physical and chemical properties at atomic level [16–19]. First-principles calculation plays a significance role for studying the grain refining mechanism and further developing of Mg alloys [20]. A growing number of researchers studied the surficial and interfacial properties by first-principles calculation to analyze the heterogeneous nucleation [21–25]. Z. Fan et al. studied the heterogeneous nucleation of Al alloys refining by Al-Ti-B-based grain refiner [21]. W. W. Xu et al. studied the Mg/MgO interfaces by first-principle calculation [22]. Li et al. and Wang et al. studied the interfacial properties of Mg/Al_4C_3 and Mg/Al_2MgC_2 interfaces by first-principles calculation, respectively [26,27]. The heterogeneous nucleation and interfacial properties are well studied using first-principles calculation method.

The adsorption model [28–30] suggests that heterogeneous nucleation is a process of melted atom adsorption on the surface of nucleation substrate in the initial nucleation process. Therefore, it is crucial to study the adsorption of melted atom on substrate surface for the study of grain refinement mechanism. In addition, several studies showed that alloy elements have a significant influence on the grain refining of metals and alloys [31–33]. It is known that alloy elements are easy to segregate to the surface and interface and affect their properties [19,34,35]. Some researches revealed that Ca element, which is a surface active element, has great influence on the grain refining effect of magnesium alloys [36–39]. It was found that Ca was segregated to the surface of nucleation substrate from our previous experiment, and Ca was easy to adsorb on substrate surfaces according to our previous calculation [39,40]. However, the effect of Ca on the grain refinement effect of carbon inoculation still need further study.

In this work, the effect of Ca on the grain refinement effect of Al_4C_3 and Al_2MgC_2 particles were studied by first-principles calculations. We analyzed the structures and properties of Ca or Mg adsorbed Al_4C_3 and Al_2MgC_2 surfaces, Ca doped Mg/Al_4C_3 and Mg/Al_2MgC_2 interfaces, respectively. The adsorption energy, the work of adhesion, the formation energy of defect and the migrate energy of the atom were investigated. Our calculated results provide a good analysis and ample support of the experimental findings, indicating that Ca is easy to adsorb on the Al_4C_3 and Al_2MgC_2 surfaces. Further, we analyzed the influence mechanism of Ca. Our work is to further explore the refinement and design of Mg alloys and provide theoretical references for them.

2. Computational details

In this paper, all calculated configurations were calculated by Vienna Ab initio Simulation Package (VASP) that based on Density functional theory (DFT) [41,42]. The projector augmented wave (PAW) method and Perdew-Burke-Ernzerhof (PBE) functional were used [43]. For the Al_2MgC_2 calculation part, the plane-wave cutoff energy was set as 400 eV, the Brillouin zone were selected as $9 \times 9 \times 5$ for the bulk calculation. For the Al_4C_3 calculation part, the plane-wave cutoff energy was set as 340 eV. We calculated the formation enthalpy of Al_4C_3 and Al_2MgC_2, which are −0.665 eV and − 0.291 eV, respectively, in line with experiment that both compounds could formed in the magnesium alloys [12,44–46]. The calculated lattice constants of Al_2MgC_2, with space group symmetry of P-3 m1 (164), are $a = 3.385$ Å and $c = 5.806$ Å, excellent agreement with the experimental lattice parameters ($a = 3.377$ Å, $c = 5.817$ Å) [47]. The Al_4C_3 bulk and surface have been analyzed in our previous work [40]. For all calculation, the Brillouin zone was selected as $4 \times 4 \times 1$ for adsorption slab and interface calculations. 20 Å was selected as the vacuum thickness and each side was 10 Å. The convergence criterion for the structural relaxation was set to 0.01 eV/Å. The climbing image nudged elastic band [48] method was used to calculate diffusion barriers for Ca atom migrate in the adsorption surface and doped interface.

3. Results and discussions

3.1. Surface properties

Since the closest packing crystal plane of Al_2MgC_2 is perpendicular to the c-axis, the surface configurations of $Al_2MgC_2(0001)$ are classified as five kinds along to c-axis direction as shown in Fig. 1 (a), including Al (Al)-, Al(C)-, C(Mg)-, C(Al)- and Mg-terminated surfaces. Al(C)-terminated surface means that the surficial layer is Al termination, and subsurface second layer is C layer, also for other surface slabs. The surface energies of different surface models were calculated by formula (1) [27] as follows:

$$\sigma_{Al_2MgC_2(0001)} = \frac{1}{2A}\left[E_{slab} - N_{Mg}\mu^{bulk}_{Al_2MgC_2} + (2N_{Mg} - N_{Al})\Delta\mu_{Al} + (2N_{Mg} - N_{Al})\mu^{bulk}_{Al} + (2N_{Mg} - N_C)\Delta\mu_C + (2N_{Mg} - N_C)\mu^{bulk}_C\right] \quad (1)$$

The E_{slab} is total energy of surface slab, N_i is the number of atom (i refers to Mg, Al and C atom, respectively), μ is the chemical potential, A represents the surface area of Al_2MgC_2 surficial slab.

In order to find the surface structure that thick enough to present bulk-like characteristic interiors, we calculated surface energies (see Fig. 1 (c) and Table 1) of different-layer slabs that belong to the same

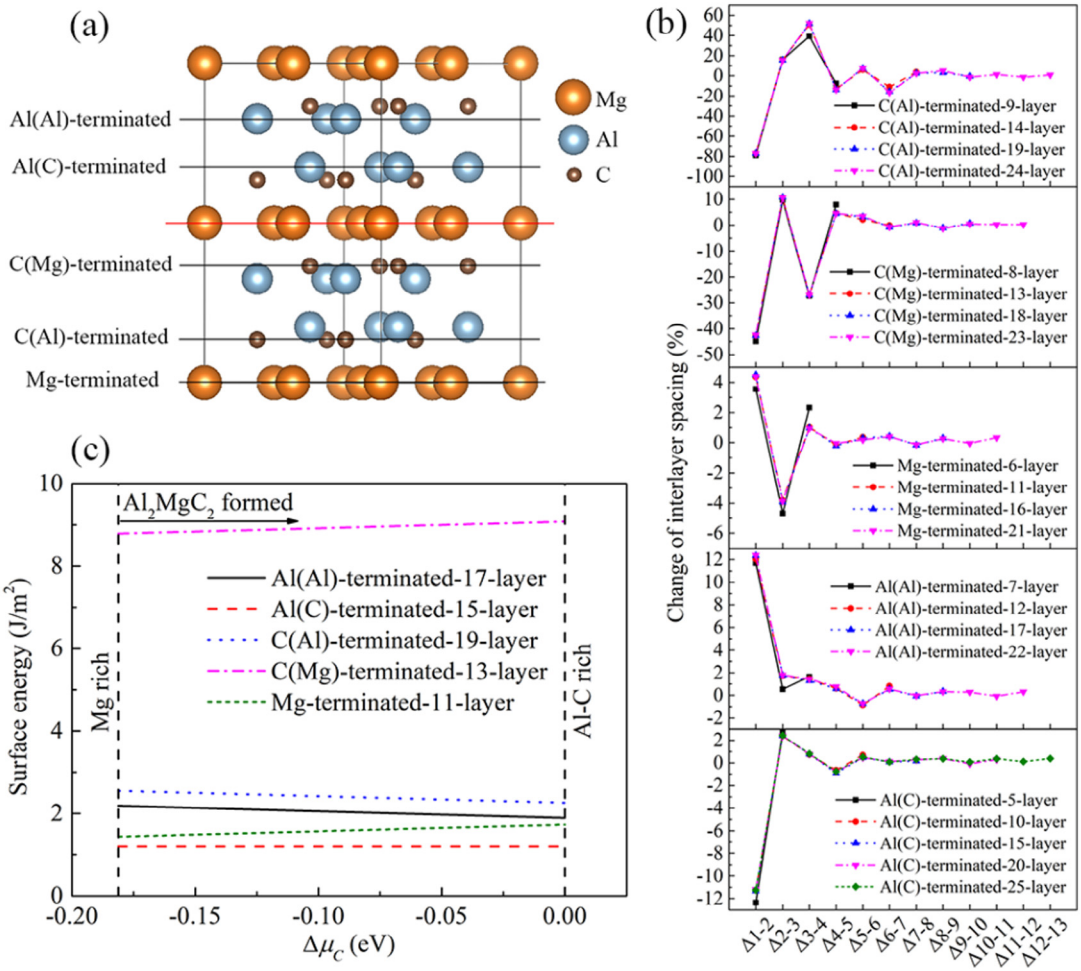

Fig. 1. (a) The schematic diagram of surface configurations of Al_2MgC_2. (b) The change of the interlayer spacing (%) of different termination surficial slabs. (c) The surface energies of Al(Al)-, Al(C)-, C(Mg)-, C(Al)- and Mg-terminated surface slabs.

configuration, also the percentage change of the interlayer spacing of different slabs (Fig. 1 (b)). From Fig. 1 (b), the change of the interlayer spacing (%) decrease and will reach convergence as the *i* and *j* of Δi-j increase. Meanwhile, the surface slab layer which reaches convergence is represented by a symbol '*' as shown in Table 1. Our calculated results of surface energies are in line with the previous results [27]. We can found that the surface energy of Al(C)-terminated-15 layers Al_2MgC_2 slab is the lowest, which also meets the stoichiometry (c.f. Fig. 1 (c)). Moreover, the change of interlayer spacing of Al(C)-terminated-15 layers slab is also reach convergence. In addition, the calculated surface energies and surface slabs of Al_4C_3 can be found in our earlier work [40], the closest packing 28-layer Al-terminated $Al_4C_3(0001)$ surface was selected. We also calculated other secondary packing surfaces of Al_2MgC_2 and Al_4C_3 structures as a test, including $Al_2MgC_2(010)$, $Al_2MgC_2(110)$, $Al_2MgC_2(111)$, $Al_4C_3(010)$ and $Al_4C_3(110)$ surfaces as shown in our supplemental material (Fig. S1, Fig. S2, Table S1 and Table S2). According to our calculation results, surface energies of Al_2MgC_2 and Al_4C_3 secondary packing surfaces are all greater than that of Al(C)-terminated-15 layers $Al_2MgC_2(001)$ slab (1.194 J/m^2) and 28-layer Al-terminated Al_4C_3 (001) surface (1.024 J/m^2). Consequently, the Al(C)-terminated-15 layers Al_2MgC_2 slab and 28-layer Al-terminated $Al_4C_3(0001)$ slab were selected for further calculation.

Table 1
Surficial energies of different Al_2MgC_2 surface structures.

Surface model	σ(J/m²)				
Al(Al)-terminated	7-layer	12-layer	17-layer *	22-layer	Δμc (eV)
	2.200	2.184	2.183	2.182	−0.181
	1.907	1.892	1.890	1.889	0
Al(C)-terminated	5-layer	10-layer	15-layer *	20-layer	Δμc (eV)
	1.215	1.196	1.194	1.193	−0.181
					0
C(Al)-terminated	9-layer	14-layer	19-layer *	24-layer	Δμc (eV)
	2.543	2.554	2.551	2.548	−0.181
	2.250	2.261	2.259	2.255	0
C(Mg)-terminated	8-layer	13-layer *	18-layer	23-layer	Δμc (eV)
	8.684	8.785	8.787	8.786	−0.181
	8.977	9.078	9.080	9.079	0
Mg-terminated	6-layer	11-layer *	16-layer	21-layer	Δμc (eV)
	1.376	1.437	1.438	1.438	−0.181
	1.668	1.729	1.731	1.731	0

The symbol * represents the layer met the convergence criterion for each kind of surface slabs.

3.2. Adsorption in the initial nucleation stage

From adsorption model, we know that atoms adsorption on crystal surfaces is significant to metal nucleation. According to EPMA-WDS mapping images of reference [40] and EPMA-BSE analysis showing as Fig. S3 and Table S3 in our supplemental material, it can be seen that Ca segregate on the surfaces of Al_2MgC_2 and Al_4C_3 particles. We

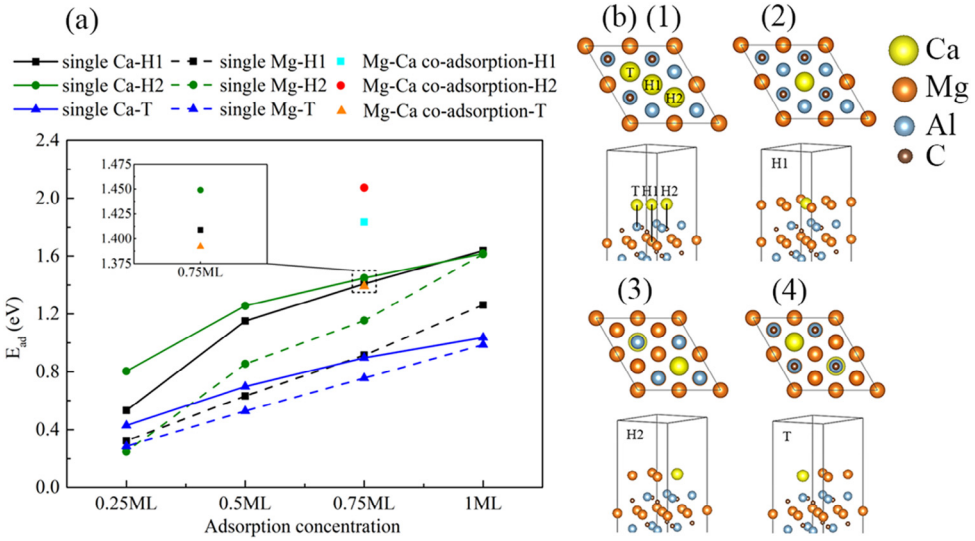

Fig. 2. (a) The E_{ad} (adsorption energy) of Ca or Mg on $Al_2MgC_2(0001)$ surficial slab. The discrete points are the E_{ad} of Mg on different sites of $Al_2MgC_2(0001)$ + Ca slabs. (b) The diagrammatic sketch of different adsorption sites that (1) single Mg or Ca adsorb $Al_2MgC_2(0001)$, (2)(3)(4) H1 site, H2 site and T site of Mg and Ca co-adsorption on $Al_2MgC_2(0001)$, respectively.

calculated the first-layer adsorption slabs of Ca/Mg on the Al_2MgC_2 and Al_4C_3 surfaces. We further calculated the second-layer adsorption of Ca/Mg on Al_2MgC_2 + 3 Mg + 1Ca, Al_2MgC_2 + 4 Mg, Al_4C_3 + 3 Mg + 1Ca and Al_4C_3 + 4 Mg surfaces, respectively, to obtain insights of initial nucleation.

The adsorption energy of i atom adsorb surficial slab is calculated by formula [34,40]:

$$E_{ad} = \left[E^{tot}_{slab1} + n_i E_i - E^{tot}_{slab2}\right]/n_i \quad (2)$$

E^{tot}_{slab1} and E^{tot}_{slab2} are the total energy of the surficial slab that before and after adsorption of i atom, respectively.

As shown in Fig. 2, the adsorption energy of H2 site is the highest, indicating that the H2 site of $Al_2MgC_2(0001)$ surface is the most stable adsorption site. According to the calculated results shown in Fig. 2, E_{ad} of Ca is significantly greater than that of Mg, therefore, Ca is easier to adsorb on $Al_2MgC_2(0001)$ surface than Mg. In addition, the E_{ad} of Mg increased because of Ca adsorption on Al_2MgC_2 (0001) surface. Calculated results revealed that Ca promotes the adsorption of Mg. Al_2MgC_2 particles attract surrounding atoms and grow up due to the presence of Ca. In our previous work [40], both Ca and Mg atoms tend to stabilize at the H2 site of Al-terminated $Al_4C_3(0001)$ surface, and Ca promotes the adsorption of Mg on Al_4C_3 surface. As shown in Fig. 3, at 0.25ML and 0.5ML coverages, E_{ad} of single Ca or Mg adsorption on Al_2MgC_2 + 3 Mg + 1Ca surface are larger, while at 0.75ML and 1ML coverages, on Al_2MgC_2 + 3 Mg + 1Ca and Al_2MgC_2 + 4 Mg surface are almost the same. The results of Ca and Mg reveal that Ca is easier to adsorb on the surface of nucleation particles. When co-adsorbed with Ca, the adsorption energy of Mg on Al_2MgC_2 + 4 Mg H1 site is the

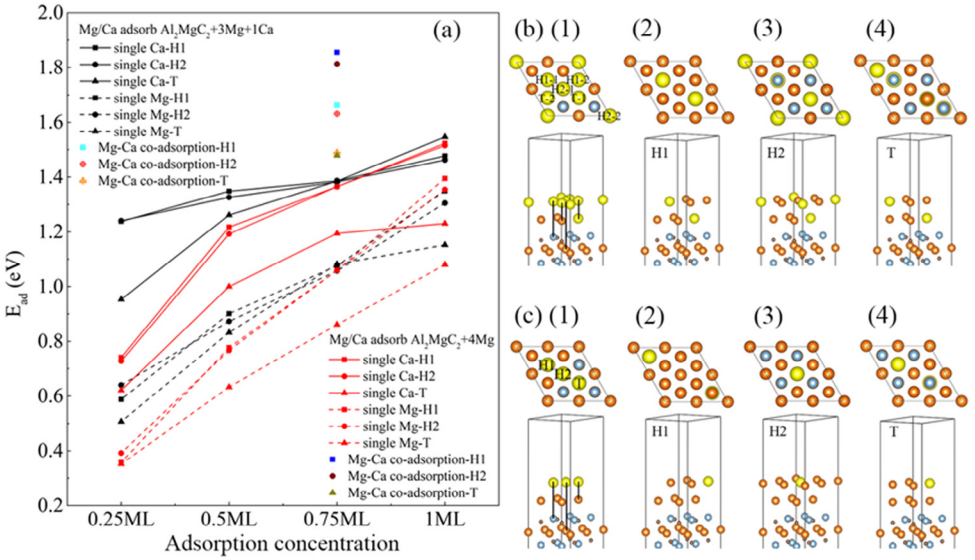

Fig. 3. (a) The E_{ad} (adsorption energy) of Ca or Mg on Al_2MgC_2 + 3 Mg + 1Ca and Al_2MgC_2 + 4 Mg slabs. (b) The diagrammatic sketch of Ca or Mg adsorb Al_2MgC_2 + 3 Mg + 1Ca that (1) single Mg or Ca adsorb $Al_2MgC_2(0001)$ slab, (2)(3)(4) H1 site, H2 site and T site of Mg and Ca co-adsorption on $Al_2MgC_2(0001)$, respectively. (c) The diagrammatic sketch of Ca or Mg adsorb Al_2MgC_2 + 4 Mg that (1) single Mg or Ca adsorb $Al_2MgC_2(0001)$ slab, (2)(3)(4) H1 site, H2 site and T site of Mg and Ca co-adsorption on $Al_2MgC_2(0001)$, respectively.

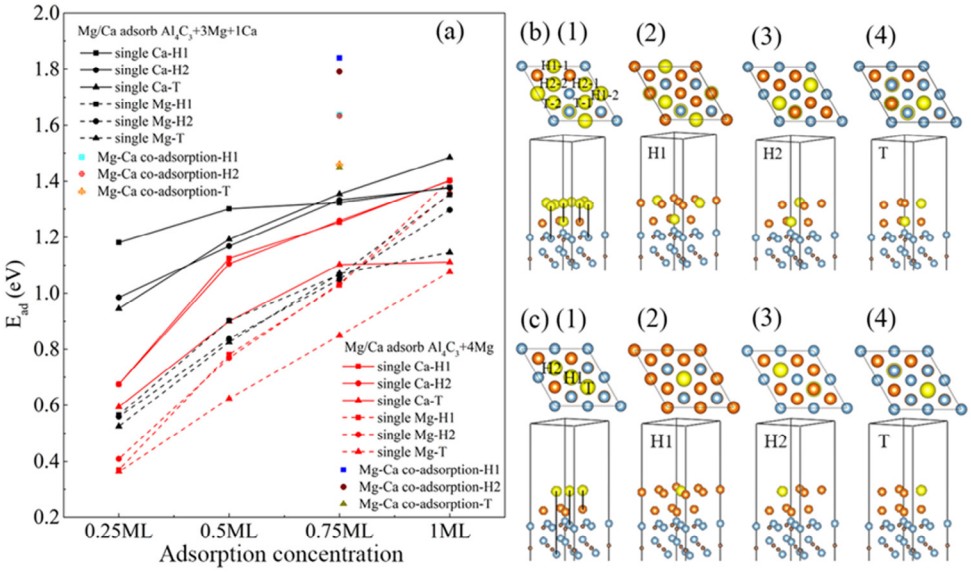

Fig. 4. (a) The E_{ad} (adsorption energy) of Ca or Mg on Al_4C_3 + 3 Mg + 1Ca and Al_4C_3 + 4 Mg slabs. (b) The diagrammatic sketch of Ca or Mg adsorb Al_4C_3 + 3 Mg + 1Ca that (1) single Mg or Ca adsorb Al_4C_3(0001), (2)(3)(4) H1 site, H2 site and T site of Mg and Ca co-adsorption on Al_4C_3(0001), respectively. (c) The diagrammatic sketch of Ca or Mg adsorb Al_4C_3 + 4 Mg that (1) single Mg or Ca adsorb Al_4C_3(0001), (2)(3)(4) H1 site, H2 site and T site of Mg and Ca co-adsorption on Al_4C_3(0001), respectively.

largest, and much larger than that of single Mg adsorption. In Fig. 4, it indicates that the adsorption energy of Ca on Al_4C_3 + 3 Mg + 1Ca surface is larger than on Al_4C_3 + 4 Mg surface. At the coverages of 0.25ML and 0.5ML, the adsorption energy of single Mg on Al_4C_3 + 3 Mg + 1Ca surface is larger, while it is almost the same on Al_4C_3 + 3 Mg + 1Ca and Al_4C_3 + 4 Mg surface at the coverage of 0.75ML and 1ML. Ca is easier to adsorption on Al_4C_3 + 3 Mg + 1Ca and Al_4C_3 + 4 Mg surface than Mg for the adsorption energies of Ca is larger. When co-adsorbed with Ca, the adsorption energy of Mg on Al_4C_3 + 4 Mg H1 site is the largest. We conclude that Ca promotes the adsorption of Mg for both first-layer and second-layer adsorption on substrate surfaces in the initial nucleation stage. This will lead to the increase of nucleation particle size and thus beneficial to the nucleation rate.

3.3. Influence of Ca on interfacial properties

3.3.1. Clean interface

According to nucleation models, the interfacial properties are important to the nucleation process. Dislocations theoretically affect the nucleation process. However, the primitive nuclei are small in the molten magnesium during actual crystallization process. If there is dislocation in primitive nuclei, it is beneficial to reduce surface mismatch stress. Moreover, the magnesium matrix is molten liquid and no dislocation effects. Therefore, dislocations are not considered in the initial nucleation stage and ideal interface structure is calculated in our work. As shown in Fig. 5 (a) and (b), we studied the W_{ad} of Mg/Al_2MgC_2 interface and Mg/Al_4C_3 interface. Interface configurations are set up as FCC (face-centered cubic), HCP (hexagonal close-packed) and OT (on the top), shown in Fig. 5 (a) and (b). In our calculation, the misfit of Mg/Al_2MgC_2 interface model is 5.7%, while that of Mg/Al_4C_3 interface model is 3.98%. In the interface slabs, atoms match well at the interface. We calculated the work of adhesion of different clean interfaces by formula as follows:

$$W_{ad}^{clean} = \frac{1}{A}\left(E_{Mg}^{slab} + E_{B}^{slab} - E_{Mg/B}^{slab}\right) \quad (3)$$

A represents the surface area of Al_2MgC_2 or Al_4C_3 surface, E_i^{slab} represents the total energy of i slab (i represents the Mg slab, Al_2MgC_2 surface slab, Al_4C_3 surface slab, Mg/Al_2MgC_2 interface slab and Mg/Al_4C_3 interface slab, respectively). It can be found that the W_{ad} of configuration HCP of Mg/Al_2MgC_2 interface and Mg/Al_4C_3 interface are both the highest, which means that these two interfaces are the most stable.

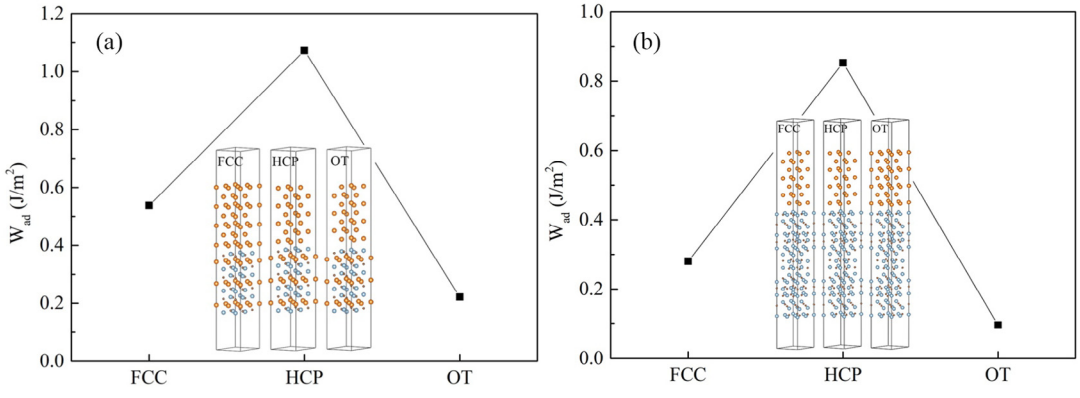

Fig. 5. (a) The work of adhesion (W_{ad}) of Mg/Al(C)-terminated Al_2MgC_2 interface. (b) The work of adhesion of Mg/Al-terminated Al_4C_3 interface.

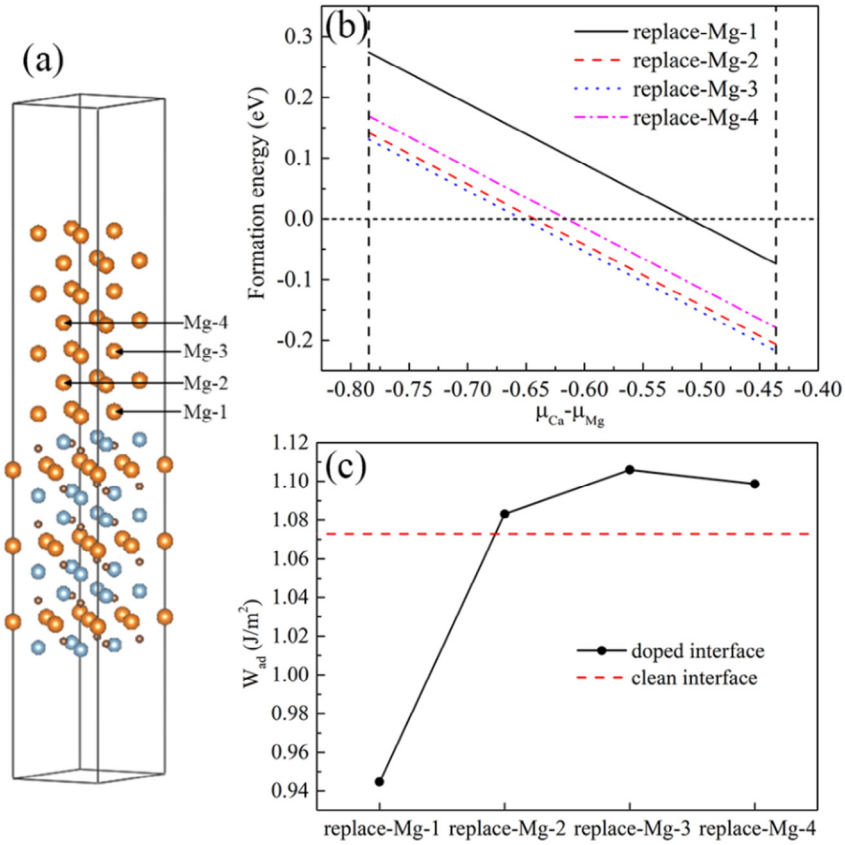

Fig. 6. (a) Schematic diagram of Mg/Al_2MgC_2 interface doping (replace-Mg-1, 2, 3 and 4 represents the site that replaced by Ca, respectively). (b) The formation energy of defect that Ca replacing different site. (c) The work of adhesion (W_{ad}) of different slabs.

Configurations HCP of Mg/Al_2MgC_2 interface and Mg/Al_4C_3 interface are employed for further Ca doping investigation.

3.3.2. Ca doped interface

From EPMA-BSE analysis showing as Fig. S3 and Table S3 in our supplemental material, it is known that the Ca content at the edge of the particle is several times that of the center of the particle. It can be regarded that Ca segregates in the interface between Al_2MgC_2/Al_4C_3 and Mg matrix. To study the effect of Ca on the interfacial properties, we calculated the Ca doped Mg/Al_2MgC_2 and Mg/Al_4C_3 interface, the formation energy of defect [49] was given by:

$$E_f = E_{\text{interface}}^{\text{doped}} - E_{\text{interface}}^{\text{clean}} - \left(\mu_{\text{Ca}} - \mu_{\text{Mg}}\right) \tag{4}$$

E_i represents the calculated energy of corresponding slab, while μ_i represents the chemical potential of the corresponding atom.

It can be seen from Fig. 6 (b) that the formation energy of Ca replacing Mg-1 slab is the largest, while that of Ca replacing Mg-2 and Mg-3 slab is smaller. According to Fig. 6 (c), the W_{ad} of Ca replacing Mg-1 slab is lower than that of clean interface, while the W_{ad} of Ca replacing Mg-2 and Mg-3 slabs are higher than that of clean interface. These indicated that Ca prefer to replace Mg-2 and Mg-3 site, which increases the stability of interface. In Fig. 7 (b), it shows that the defect formation energy of Ca replacing Mg-2 slab is the lowest. From Fig. 7 (c), we know that W_{ad} of Ca replacing Mg-2 slab is the largest and larger than W_{ad} of the clean interface. This means that Ca is easily to replace Mg-2 site and enhance the adhesion of Mg/Al_4C_3 interface. According to the above analysis, it concludes that Ca is difficult to replace Mg-1, while it is stable and easy to replace Mg-2, on both Mg/Al_2MgC_2 interface and Mg/Al_4C_3 interface. Combining the analysis of adsorption in the initial nucleation stage, it infers that Ca will preferentially adsorb on the surface of the Al_2MgC_2 and Al_4C_3 particles in the initial stage of nucleation. However, in the process of forming the interface in the later stage of nucleation, Ca is unstable in the first layer and may migrate from the first layer to the second layer, thereby making the structure stable. We will discuss the possible diffusion between the first and second layers in the following.

3.4. Diffusion paths and related electronic properties

To study the diffusion route and energy barrier of Ca atom, we analyze two scenarios, i.e., adsorption model and interface doping model. We constructed the initial, final and some intermediate configurations that contains one Mg vacancy, and the CI-NEB (climbing image nudged elastic band) optimized configurations are shown in Fig. 8.

The Mg vacancy formation energy was calculated by formula:

$$\Delta H^f\left(V_{\text{Mg}}\right) = E' + \mu_{\text{Mg}} - E_0 \tag{5}$$

The E' is the total energy of vacancy defect structure, E_0 is the total energy of ideal structure without vacancy. μ_{Mg} is the chemical potential of Mg atom, $\mu_{\text{Mg}} = E_{\text{Mg}}^{\text{bulk}}/n_{\text{Mg}}$ for the nucleation process is in the environment of the molten magnesium.

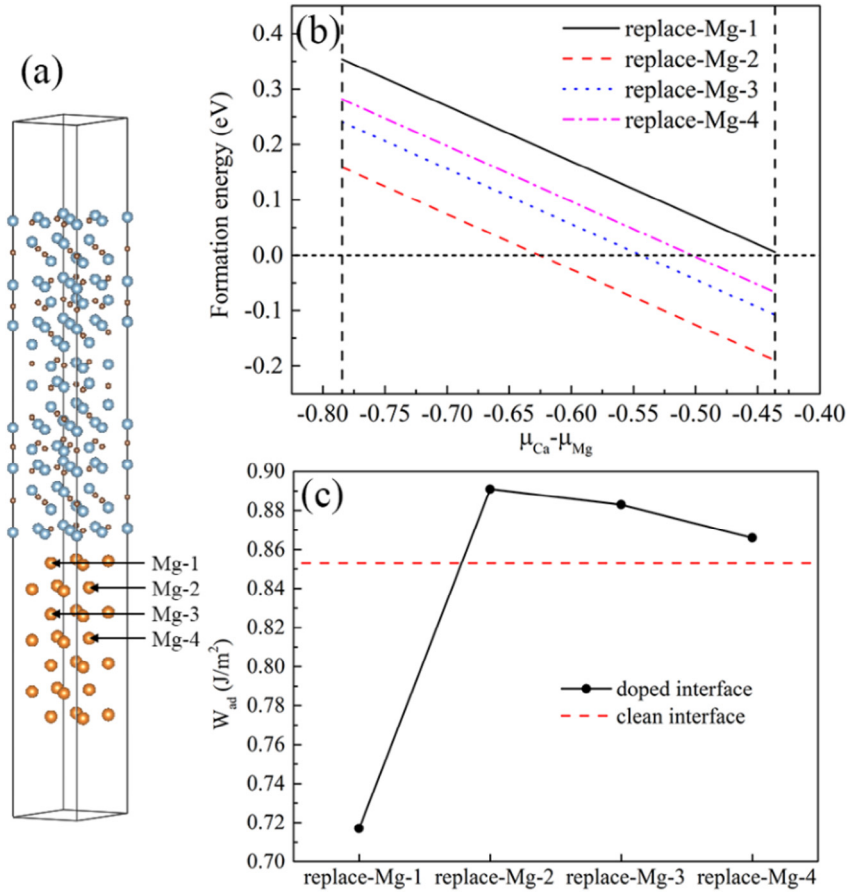

Fig. 7. (a) Schematic diagram of Mg/Al_4C_3 interface doping (replace-Mg-1, 2, 3 and 4 represents the site that replaced by Ca, respectively). (b) The formation energy of defect that Ca replacing different site. (c) The work of adhesion (W_{ad}) of different slabs.

The vacancy concentration can be estimated according to the formula [50]:

$$C_{Va} = A_{Va}^{C} \cdot \exp\left(-\frac{H_{Va}^{F}}{k_B T}\right) \quad (6)$$

A_{Va}^{C}, H_{Va}^{F} and k_B represent the Mg site concentration, vacancy formation energy, and Boltzmann constant, respectively. T is the corresponding experimental temperature, and is set to 1033.15 K [40,51].

According to formula (5) and (6), the calculated vacancy concentration of the Al_2MgC_2 adsorption slab is $7.92 \times 10^{19}/cm^3$, and correspondingly $9.41 \times 10^{20}/cm^3$ for Mg/Al_2MgC_2 doped interface slab, $2.60 \times 10^{19}/cm^3$ for Al_4C_3 adsorption slab and $1.87 \times 10^{19}/cm^3$ for Mg/Al_4C_3 doped interface slab, respectively. According to the calculated vacancy formation energy and vacancy concentration of Mg vacancy, it can be concluded that the Mg vacancy is rather easy to form. As shown in Fig. 8, the energy barrier of Ca adsorbed Al_2MgC_2 slab and Ca doped Mg/Al_2MgC_2 interface are 0.510 eV and 0.471 eV, respectively. The energy barrier of Ca adsorbed Al_4C_3 slab and Ca doped Mg/Al_4C_3 interface are 0.492 eV and 0.449 eV, respectively. All these calculated diffusion barrier are acceptable, indicating that Ca can migrate from the first layer to the second layer. Combined with the analysis of adsorption results, it can be concluded that Ca will adsorb on Al_2MgC_2 and Al_4C_3 surface at the initial stage of nucleation, then migrate from the adsorption first layer to the adsorption second layer as the nucleus grows up. It also can migrate from the first layer to the second layer at the process of interface forming.

We analyzed the charge difference density and Electron Localization Function (ELF) [52] for the initial and final states of different configurations, respectively. As defined in reference [52], the value of ELF is between 0 and 1, corresponding to completely delocalized and fully localized electronic configurations. As shown in Fig. 9, the charge is distributed throughout the space around adsorbed Mg atoms and Ca atoms on the adsorption surface, showing the feature of metal bonding. According to the charge density difference and local charge distribution, charges are accumulated around the surficial C atoms, while there is little charge around the adsorption Mg atoms according to ELF results. This reveals that the adsorbed atoms formed mixed ion/covalent bonds with the surficial C atoms. The charge around Ca atoms is more localized than other atoms. It formed the ionic bond between the Ca and C atom, while formed mixed metal/covalent bond between the Ca and surrounding atoms in the initial state of adsorption slab and doping slab. According to the 3D charge difference density and ELF, there exists more charge between Ca and Mg in the initial state in contrast to the final state. The adsorption of Ca causes changes in surface properties, and the surficial charge is redistributed, possibly leading to the fact that Mg is more easily adsorbed.

3.5. Analysis of influence mechanism of Ca

According to the metal crystallization thermodynamics, only the crystal nucleus that reached the critical nucleation radius (r_K

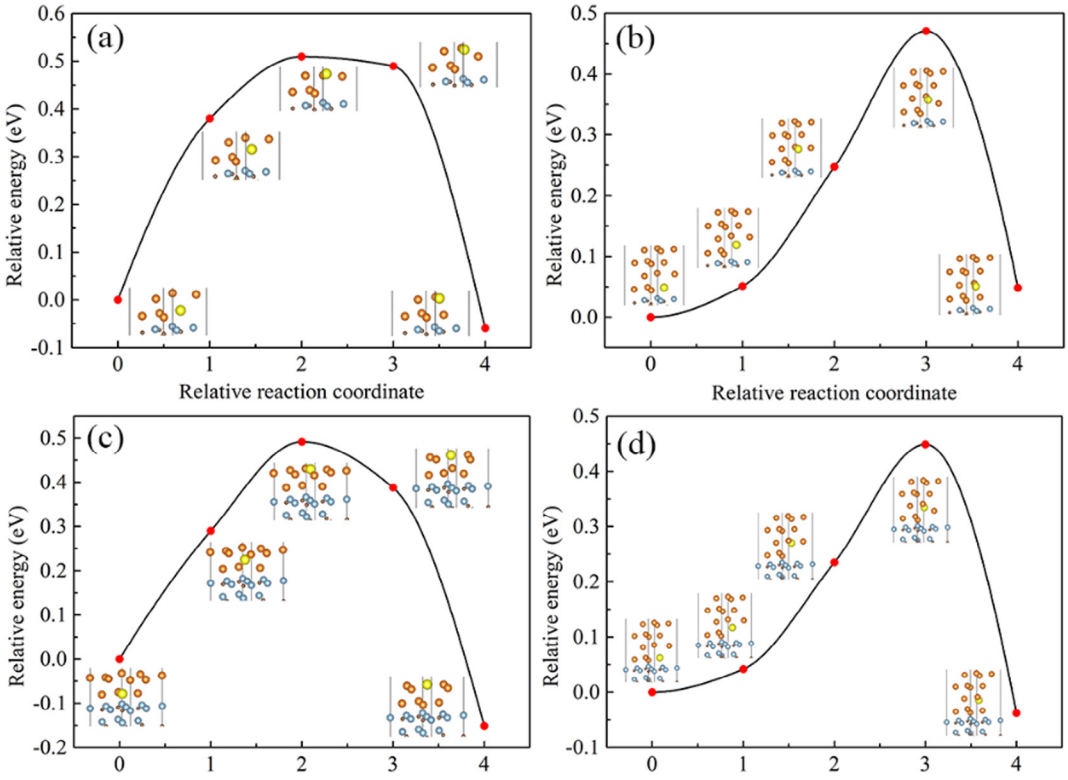

Fig. 8. Diffusion route and energy barrier of Ca atom are shown, including the initial, final and some intermediate configurations in the transition process. (a) Slab of Ca and Mg adsorb Al_2MgC_2 surface, (b) Slab of Ca doped Mg/Al_2MgC_2 interface, (c) Slab of Ca and Mg adsorb Al_4C_3 surface, (d) Slab of Ca doped Mg/Al_4C_3 interface.

$= \frac{2\sigma_{\alpha L}T_m}{\Delta H_f \Delta T}$) can exist stably in melt and continue to grow, eventually becoming an effective crystal grain. According to all the above analysis, the adsorption energy of Ca on Al_2MgC_2 and Al_4C_3 surfaces is significant greater than that of Mg, Ca adsorbs first and then improves the adsorption of Mg on these particles. Therefore, Al_2MgC_2 and Al_4C_3 particles are more easily to attract the adsorption of surrounding Mg atoms and grow up. Some Al_2MgC_2 and Al_4C_3 particles in the molten Mg alloys are big enough that their radius is larger than r_K and they can play a good role in heterogeneous nucleation. Moreover, there always have some Al_2MgC_2 and Al_4C_3 particles with a radius slightly smaller than the critical nucleation radius. As shown in Fig. 10, we suppose that the radius of primary Al_2MgC_2 and Al_4C_3 particles is r_{K1}, and the critical nucleation radius is r_K. If the r_{K1} is less than but close to r_K, with the adsorption of Ca and its assisting adsorption of Mg, the radius of these Al_2MgC_2 and Al_4C_3 particles will increase to r_{K2}, which is larger than r_K. Based on the diffusion investigation in our work, Ca will migrate from the surficial first layer to surficial second layer during the process of initial nucleation, as describes in Fig. 10. After Ca diffusion to the surficial second layer, Ca will still further promote the adsorption of Mg on surface of substrate particles. In summary, the radius of more particles will larger than r_K because of Ca. As a result, the number of effective nucleation particles increases and followed by the nucleation rate due to the influence of Ca. In addition, Ca makes the Mg/Al_2MgC_2 and Mg/Al_4C_3 interfaces more stable, it is beneficial to the grain refining.

4. Conclusions

We have studied the influence mechanism of Ca element on grain refining of carbon-inoculated Mg—Al alloy by first-principles calculation. Our studies and analysis are instructive for the design and development of magnesium metals and alloys. The main findings are listed as follows:

(1) E_{ad} of Ca on Al_2MgC_2 and Al_4C_3 surfaces is significant greater than that of Mg for both first-layer and second-layer adsorption. Al_2MgC_2 and Al_4C_3 particles are more easily to adsorb surrounding molten Mg atoms and grow up due to the adsorbed Ca.
(2) Configurations HCP of Mg/Al_2MgC_2 and Mg/Al_4C_3 interfaces are both the most stable. Ca enhances the stability of Mg/Al_2MgC_2 and Mg/Al_4C_3 interfaces, as W_{ad} of Ca replaced Mg-2 interfaces are greater than that of corresponding clean interfaces.
(3) Ca can migrate from surficial first-layer to surficial second-layer in the initial stage of nucleation. After Ca diffusion to the surficial second layer, it still promotes the adsorption of Mg.
(4) Because of the influence of Ca, the radius (r_{K1}) of more particles could increase to r_{K2} and beyond the critical nucleation radius r_K, therefore, more particles act as the effective nucleation. As a result, the nucleation rate increase and thus improves the grain refinement of Mg—Al alloys.

CRediT authorship contribution statement

Shu-Qing Yang: Formal analysis, Writing - original draft. **Cheng-Bo Li:** Formal analysis. **Jun Du:** Supervision, Writing - review & editing. **Yu-Jun Zhao:** Supervision, Writing - review & editing.

Declaration of competing interest

The authors declare that they have no known competing financial interests or personal relationships that could have appeared to influence the work reported in this paper.

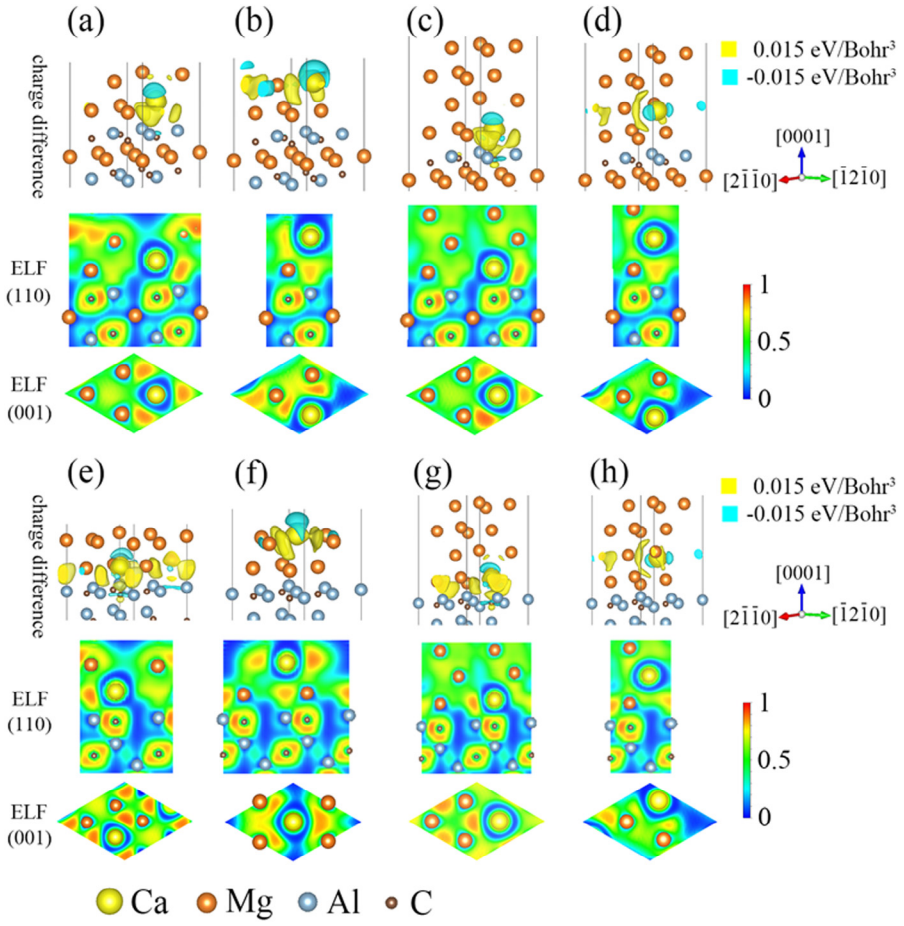

Fig. 9. The 3D charge difference density and the cross section and longitudinal section ELF through the Ca atom. (a) (b) The initial and final state of Ca adsorbed Al_2MgC_2 surface, respectively. (c) (d) The initial and final state of Ca doped Mg/Al_2MgC_2 interface, respectively. (e) (f) The initial and final state of Ca adsorbed Al_4C_3 surface, respectively. (g) (h) The initial and final state of Ca doped Mg/Al_4C_3 interface, respectively.

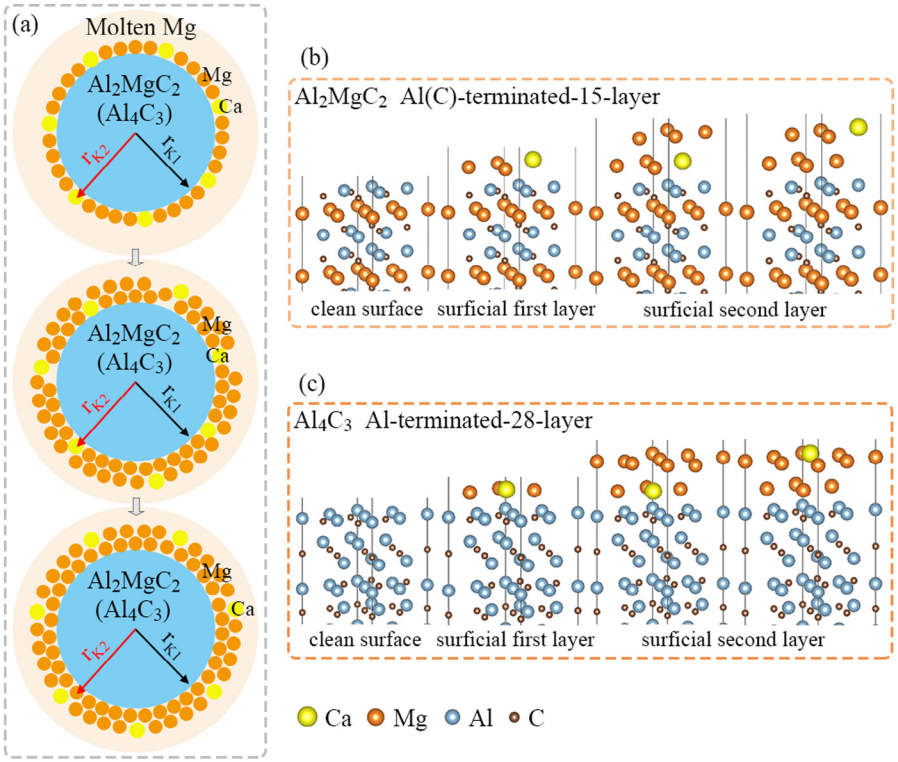

Fig. 10. (a) The schematic diagram of initial nucleation progress. (b) The clean surface and adsorption slabs of Al_2MgC_2. (c) The clean surface and adsorption slabs of Al_4C_3.

Acknowledgments

This work was supported by the National Natural Science Foundation of China (51574127, 11574088) and Natural Science Foundation of Guangdong Province (2014A030313221).

Appendix A. Supplementary data

Supplementary data to this article can be found online at https://doi.org/10.1016/j.matdes.2020.108664.

References

[1] M. Gupta, N. Gupta, The promise of magnesium based materials in aerospace sector, Int. J. Aeronautics Aerospace Res. 4 (2017) 141–149, https://doi.org/10.19070/2470-4415-1700017.
[2] S.H. You, Y.D. Huang, K.U. Kainer, N. Hort, Recent research and developments on wrought magnesium alloys, J. Magnes. Alloy 5 (2017) 239–253, https://doi.org/10.1016/j.jma.2017.09.001.
[3] A.A. Luo, Magnesium casting technology for structural applications, J. Magnes. Alloy 1 (2013) 2–22, https://doi.org/10.1016/j.jma.2013.02.002.
[4] T.C. Xu, Y. Yang, X.D. Peng, J.F. Song, F.S. Pan, Overview of advancement and development trend on magnesium alloy, J. Magnes. Alloy 7 (2019) 536–544, https://doi.org/10.1016/j.jma.2019.08.001.
[5] X.J. Wang, D.K. Xu, R.Z. Wu, X.B. Chen, Q.M. Peng, L. Jin, Y.C. Xin, Z.Q. Zhang, Y. Liu, X.H. Chen, G. Chen, K.K. Deng, H.Y. Wang, What is going on in magnesium alloys? J. Mater. Sci. Technol. 34 (2017) 245–247, https://doi.org/10.1016/j.jmst.2017.07.019.
[6] H.H. Yu, Y.C. Xin, M.Y. Wang, Q. Liu, Hall-Petch relationship in Mg alloys: a review, J. Mater. Sci. Technol. 34 (2018) 248–256, https://doi.org/10.1016/j.jmst.2017.07.022.
[7] D. Turnbull, Kinetics of heterogeneous nucleation, J. Chem. Phys. 18 (1950) 198–203, https://doi.org/10.1063/1.1747588.
[8] Y. Ali, D. Qiu, B. Jiang, F.S. Pan, M.X. Zhang, Current research progress in grain refinement of cast magnesium alloys: a review article, J. Alloy. Compd. 619 (2015) 639–651, https://doi.org/10.1016/j.jallcom.2014.09.061.
[9] M. Qian, P. Cao, Discussions on grain refinement of magnesium alloys by carbon inoculation, Scripta Mater 52 (2005) 415–419, https://doi.org/10.1016/j.scriptamat.2004.10.014.
[10] M. Suresh, A. Srinivasan, U.T.S. Pillai, B.C. Pai, The effect of charcoal addition on the grain refinement and ageing response of magnesium alloy AZ91, Mat. Sci. Eng. A 528 (2011) 8573–8578, https://doi.org/10.1016/j.msea.2011.08.004.
[11] S. Nimityongskul, M. Jones, H. Choi, R. Lakes, S. Kou, X.C. Li, Grain refining mechanisms in Mg-Al alloys with Al_4C_3 microparticles, Mat. Sci. Eng. A 527 (2010) 2104–2111, https://doi.org/10.1016/j.msea.2009.12.030.
[12] Y.D. Huang, K.U. Kainer, N. Hort, Mechanism of grain refinement of Mg-Al alloys by SiC inoculation, Scripta Mater 64 (2011) 793–796, https://doi.org/10.1016/j.scriptamat.2011.01.005.
[13] D. Turnbull, B. Vonnegut, Nucleation catalysis, Ind. Eng. Chem. 44 (1952) 1292–1298, https://doi.org/10.1021/ie50510a031.
[14] B.L. Bramfitt, The effect of carbide and nitride additions on the heterogeneous nucleation behavior of liquid iron, Metall. Trans. 1 (1970) 1987–1995, https://doi.org/10.1007/BF03037838.
[15] M.X. Zhang, P.M. Kelly, Crystallography and morphology of widmanstätten cementite in austenite, Acta Mater. 46 (1998) 4617–4628, https://doi.org/10.1016/S1359-6454(98)00139-6.
[16] H.G. Yang, C.H. Sun, S.Z. Qiao, J. Zou, G. Liu, S.C. Smith, H.M. Cheng, G.Q. Lu, Anatase TiO_2 single crystals with a large percentage of reactive facets, Nature 453 (2008) 638–641, https://doi.org/10.1038/nature06964.
[17] S. Lu, Q.M. Hu, R. Yang, B. Johansson, L. Vitos, First-principles determination of the α-α' interfacial energy in Fe-Cr alloys, Phys. Rev. B 82 (2010), 195103. https://doi.org/10.1103/PhysRevB.82.195103.
[18] H. Zhang, S.L. Shang, Y. Wang, A. Saengdeejing, L.Q. Chen, Z.K. Liu, First-principles calculations of the elastic, phonon and thermodynamic properties of $Al_{12}Mg_{17}$, Acta Mater. 58 (2010) 4012–4018, https://doi.org/10.1016/j.actamat.2010.03.020.
[19] Z.R. Pei, R. Li, J.F. Nie, J.R. Morris, First-principles study of the solute segregation in twin boundaries in Mg and possible descriptors for mechanical properties, Mater. Des. 165 (2019), 107574. https://doi.org/10.1016/j.matdes.2018.107574.
[20] D.W. Shin, C. Wolverton, First-principles density functional calculations for Mg alloys: a tool to aid in alloy development, Scripta Mater 63 (2010) 680–685, https://doi.org/10.1016/j.scriptamat.2009.12.032.
[21] Z. Fan, Y. Wang, Y. Zhang, T. Qin, X.R. Zhou, G.E. Thompson, T. Pennycook, T. Hashimoto, Grain refining mechanism in the Al/Al-Ti-B system, Acta Mater. 84 (2015) 292–304, https://doi.org/10.1016/j.actamat.2014.10.055.
[22] W.W. Xu, A.P. Horsfield, D. Wearing, P.D. Lee, First-principles calculation of Mg/MgO interfacial free energies, J. Alloy. Compd. 650 (2015) 228–238, https://doi.org/10.1016/j.jallcom.2015.07.289.
[23] S.Q. Yang, J. Du, Y.J. Zhao, First-principles study of ZnO/Mg heterogeneous nucleation interfaces, Mater. Res. Express 5 (2018), 036519. https://doi.org/10.1088/2053-1591/aab41f.
[24] X.W. Fan, B. Chen, M.M. Zhang, D. Li, Z. Liu, C.Y. Xiao, First-principles calculations on bonding characteristic and electronic property of TiC(111)/TiN(111) interface, Mater. Des. 112 (2016) 282–289, https://doi.org/10.1016/j.matdes.2016.09.053.
[25] L. Chen, Y.F. Li, B. Xiao, Q.L. Zheng, Y.M. Gao, S.Y. Zhao, Z.C. Wang, First-principles calculation on the adhesion strength, fracture mechanism, interfacial bonding of the NiTi(111)//α-Al_2O_3(0001) interfaces, Mater. Des. 183 (2019), 108119. https://doi.org/10.1016/j.matdes.2019.108119.
[26] K. Li, Z.G. Sun, F. Wang, N.G. Zhou, X.W. Hu, First-principles calculations on Mg/Al_4C_3 interfaces, Appl. Surf. Sci. 270 (2013) 584–589, https://doi.org/10.1016/j.apsusc.2013.01.089.
[27] H.L. Wang, J.J. Tang, Y.J. Zhao, J. Du, First-principles study of Mg/Al_2MgC_2 heterogeneous nucleation interfaces, Appl. Surf. Sci. 355 (2015) 1091–1097, https://doi.org/10.1016/j.apsusc.2015.04.046.
[28] W.T. Kim, B. Cantor, An adsorption model of the heterogeneous nucleation of solidification, Acta Metall. Mater. 42 (1994) 3115–3127, https://doi.org/10.1016/0956-7151(94)90409-X.
[29] A. Dabrowski, Adsorption—from theory to practice, Adv. Colloid Interfac. 93 (2001) 135–224, https://doi.org/10.1016/s0001-8686(00)00082-8.
[30] B. Cantor, Heterogeneous nucleation and adsorption, Phil. Trans. R. Soc. Lond. A 361 (2003) 409–417, https://doi.org/10.1098/rsta.2002.1137.
[31] Y.C. Lee, A.K. Dahle, D.H. St John, The role of solute in grain refinement of magnesium, Metall. Mater. Trans. A 31A (2000) 2895–2906, https://doi.org/10.1007/BF02830349.
[32] T.E. Quested, A.T. Dinsdale, A.L. Greer, Thermodynamic modelling of growth-restriction effects in aluminium alloys, Acta Mater. 53 (2005) 1323–1334, https://doi.org/10.1016/j.actamat.2004.11.024.
[33] H. Men, Z. Fan, Effects of solute content on grain refinement in an isothermal melt, Acta Mater. 59 (2011) 2704–2712, https://doi.org/10.1016/j.actamat.2011.01.008.
[34] A.C.P. Jain, D.R. Trinkle, First principles calculations of beryllium stability in zirconium surfaces, Acta Mater. 122 (2017) 359–368, https://doi.org/10.1016/j.actamat.2016.10.003.
[35] C.Q. Liu, H.W. Chen, N.C. Wilson, J.F. Nie, Zn segregation in interface between $Mg_{17}Al_{12}$ precipitate and Mg matrix in Mg-Al-Zn alloys, Scripta Mater 163 (2019) 91–95, https://doi.org/10.1016/j.scriptamat.2019.01.001.
[36] J. Yang, J. Peng, E.A. Nyberg, F.S. Pan, Effect of Ca addition on the corrosion behavior of Mg-Al-Mn alloy, Appl. Surf. Sci. 369t (2016) 92–100, https://doi.org/10.1016/j.apsusc.2016.01.283.
[37] J. Du, J. Yang, M. Kuwabara, W.F. Li, J.H. Peng, Improvement of grain refining efficiency for Mg-Al alloy modified by the combination of carbon and calcium, J. Alloy. Compd. 470 (2009) 134–140, https://doi.org/10.1016/j.jallcom.2008.02.052.
[38] B.C. Zhou, S.L. Shang, Y. Wang, Z.K. Liu, Diffusion coefficients of alloying elements in dilute Mg alloys: a comprehensive first-principles study, Acta Mater. 103 (2016) 573–586, https://doi.org/10.1016/j.actamat.2015.10.010.
[39] C.B. Li, C. Wen, J. Du, W.F. Li, M.Y. Zhan, Inoculant fading-resistance of Fe-bearing Mg-3%Al alloys refined by carbon combining with calcium addition, Mater. Trans. 59 (2018) 1878–1886, https://doi.org/10.2320/matertrans.M2018208.
[40] S.Q. Yang, C.B. Li, J. Du, Y.J. Zhao, Influence of Ca adsorption on the heterogeneous nucleation of α-Mg on Al_4C_3 particles: first-principles calculation and experiment, Appl. Surf. Sci. 491 (2019) 187–194, https://doi.org/10.1016/j.apsusc.2019.06.140.
[41] A.K. Rajagopal, J. Callaway, Inhomogeneous electron gas, Phys. Rev. B 7 (1973) 1912–1919, https://doi.org/10.1103/PhysRevB.7.1912.
[42] G. Kresse, J. Furthmüller, Efficient iterative schemes for ab initio total-energy calculations using a plane-wave basis set, Phys. Rev. B 54 (1996) 11169–11186, https://doi.org/10.1103/physrevb.54.11169.
[43] P.E. Blöchl, Projector augmented-wave method, Phys. Rev. B 50 (1994) 17953–17979, https://doi.org/10.1103/PhysRevB.50.17953.
[44] S.F. Liu, Y. Chen, H. Han, Grain refinement of AZ91D magnesium alloy by a new Mg-50%Al_4C_3 master alloy, J. Alloy. Compd. 624 (2015) 266–269, https://doi.org/10.1016/j.jallcom.2009.12.064.
[45] M. Suresh, A. Srinivasan, U.T.S. Pillai, B.C. Pai, Mechanism for grain refinement and mechanical properties of AZ91 Mg alloy by carbon inoculation, Procedia Eng 55 (2013) 93–97, https://doi.org/10.1016/j.proeng.2013.03.225.
[46] M.X. Han, X.Z. Zhu, T. Gao, X.F. Liu, Revealing the roles of Al_4C_3 and Al_8Mn_5 during α-mg nucleation in mg-Al based alloys, J. Alloy. Compd. 705 (2017) 14–21, https://doi.org/10.1016/j.jallcom.2017.02.116.
[47] F. Bosselet, B.F. Mentzen, J.C. Viala, M.A. Etoh, J. Bouix, Synthesis and structure of T2-Al_2MgC_2, Eur. J. Solid State Inorg. Chem. 35 (1998) 91–99, https://doi.org/10.1002/chin.199828008.
[48] G. Henkelman, B.P. Uberuaga, H. Jónsson, A climbing image nudged elastic band method for finding saddle points and minimum energy paths, J. Chem. Phys. 113 (2000) 9901–9904, https://doi.org/10.1063/1.1329672.
[49] S.K. Nayak, C.J. Hung, V. Sharma, S.P. Alpay, A.M. Dongare, W.J. Brindley, R.J. Hebert, Insight into point defects and impurities in titanium from first principles, npj Comput. Mater. 4 (2018) 11, https://doi.org/10.1038/s41524-018-0068-9.
[50] S.L. Shang, B.C. Zhou, W.Y. Wang, A.J. Ross, X.L. Liu, Y.J. Hu, H.Z. Fang, Y. Wang, Z.K. Liu, A comprehensive first-principles study of pure elements: vacancy formation and migration energies and self-diffusion coefficients, Acta Mater. 109 (2016) 128–141, https://doi.org/10.1016/j.actamat.2016.02.031.
[51] C.B. Li, S.Q. Yang, G. Luo, H.B. Liao, J. Du, Revealing the nuclei formation in carbon-inoculated Mg-3%Al alloys containing trace Fe, Materials 12 (2019) 2478, https://doi.org/10.3390/ma12152478.
[52] A.D. Becke, K.E. Edgecombe, A simple measure of electron localization in atomic and molecular systems, J. Chem. Phys. 92 (1990) 5397–5403, https://doi.org/10.1063/1.458517.